Development and testing of a rapid, sensitive, high-resolution tool to improve mapping of CO_2 leakage at the ground surface

Stefano Graziani[a], *Stan E. Beaubien*[a*], *Giancarlo Ciotoli*[b], *Sabina Bigi*[a]

[a]Dipartimento di Scienze della Terra, Università di Roma "La Sapienza", Piazzale Aldo Moro 5, Rome 00185, Italy

stefano.graziani@uniroma1.it; stanley.beaubien@uniroma1.it; sabina.bigi@uniroma1.it

[b]Istituto di Geologia Ambientale e Geoingegneria del Consiglio Nazionale delle Ricerche, Via Salaria km 29.300, Monterotondo 00015, Italy.

giancarlo.ciotoli@igag.cnr.it

[*] Corresponding author: Stan E. Beaubien (stanley.beaubien@uniroma1.it)

Abstract

Locating and quantifying anomalous, deep-origin CO_2 leakage from the soil to the atmosphere is typically accomplished by interpolating a dataset of point flux measurements, with overall accuracy and uncertainty strongly influenced by sample spacing relative to anomaly size and variability. To reduce this uncertainty we have developed the Ground CO_2 Mapper, a low-cost complementary tool that rapidly measures, at high spatial resolution, the distribution of CO_2 concentration at the ground-air contact as a proxy of CO_2 flux. Laboratory tests show that the Mapper has a low noise level (2σ = 16 ppm) and fast response time (T_{90} = 1.55 seconds), while field tests at a small controlled-release site define a high level of reproducibility and sensitivity and illustrate the impact of wind and survey speed on instrument response. Modelling based on these results indicates that the Mapper has a greater than 60% probability of detecting an intersected 2 m wide anomaly having a maximum CO_2 flux rate of 75 and 100 g m^{-2} d^{-1} at survey speeds of 2.5 and 4.8 km hr^{-1}, respectively, under the test conditions. Measurements in a large (4600 m^2) field where natural geogenic CO_2 is leaking show how the Mapper can produce, in <10% of the time, a more detailed map of CO_2 flux distribution than a point flux survey conducted on a ca. 10 m grid spacing grid. Based on these results we believe the Ground CO_2 Mapper can give a useful contribution to diffuse degassing studies in volcanic / geothermal areas and to monitoring of Carbon Capture and Storage (CCS) sites by reducing overall survey time, costs and uncertainty.

Keywords: diffuse degassing, CCS, CO_2 flux, soil gas, leakage mapping, uncertainty

1. INTRODUCTION

In most geological settings the only significant source of CO_2 flux from the ground surface to the atmosphere comes from biological respiration in the soil (Oertel et al., 2016), with spatial and temporal variability controlled by water content, temperature, organic matter content, and other environmental factors (Barron-Gafford et al., 2011). There is the potential, however, that the leakage of deeper origin CO_2 can be superimposed on this background, as occurs in geothermal / volcanic areas (Werner et al., 2019) and could potentially occur, even if unlikely, above Carbon Capture and Storage (CCS) sites (Jenkins, 2020). The study of such anomalous fluxes is important to: i) map its distribution to understand the underlying migration pathways (e.g., faults; Bigi et al., 2014); ii) quantify the total amount to determine, for example, heat flow in geothermal areas (Chiodini et al., 2021), carbon loading to the atmosphere, or CCS storage integrity / carbon credit auditing (Gal et al., 2019; Shao et al., 2019); and iii) assess any potential leakage-related risks to human health or the local ecosystem (West et al., 2015).

The magnitude, form and spatial distribution of natural CO_2 leaks depend on near-surface geological conditions and whether diffusive or advective flow predominates (Roberts et al., 2015). If vertical diffusion predominates, for example from degassing of a shallow, CO_2-saturated aquifer, leakage flux rates are lower and distribution tends to be more dispersed (Chiodini et al., 2004). If, instead, vertical permeability pathways allow for direct, pressure-driven advective flow to the surface, CO_2 leakage tends to be concentrated in a series of small, high-flux areas (gas vents) that are surrounded by lower flux haloes caused by horizontal diffusion in the unsaturated zone (Annunziatellis et al., 2008a; Oldenburg et al., 2010); vent halos may merge if gas vents are sufficiently close to each other. In the unlikely event of leakage from a CCS reservoir, this latter style would predominate (e.g., Jones et al., 2014) given that vertical diffuse leakage can only be established over very long time periods.

Mapping and quantification of leakage flux typically involves making numerous point flux measurements (limited by time/budget/logistical constraints) using the accumulation chamber method (Kutzbach et al., 2007), and then applying statistical and geostatistical tools to interpolate and interpret the results (Cardellini et al., 2003; Lewicki et al., 2005; Elío et al., 2016; Schroder et al., 2017). If spot leakage is the dominant process, however, Monte Carlo simulations have shown how sample spacing and strategy (relative to anomaly size, shape and orientation) can have a significant impact on the probability of finding leaks and on the uncertainty of any flux quantification estimates (Beaubien et al., 2021).

The availability of additional high-density data that outlines the location and extent of spot leakage prior to making flux measurements would greatly minimize these uncertainties. To address this, the present authors first proposed the idea of using a mobile platform to map the distribution of CO_2 at the ground-atmosphere contact (Annunziatellis et al., 2008b; Jones et al. 2009), an interval where CO_2 can accumulate above leakage areas due to its greater density relative to air and reduced wind mixing (Oldenburg and Unger, 2004). Although this prototype suffered from very slow response and wash-out times, and thus poor sensitivity and smeared anomalies, the results showed the potential of the approach (Jones et al. 2009). In particular, sampling at different heights above a gas leakage point showed much higher concentrations in direct contact with the ground compared to even a 10 cm offset (where wind mixing caused significant dilution). Other researchers have subsequently tested mobile CO_2 mapping tools for CCS applications, however these studies involved drawing gas at greater heights above the ground (10 - 80 cm) to protect the large and expensive spectrometers that were used (Krevor et al., 2010; Feitz et al., 2018; Barkwith et al., 2020). CO_2 sensors have also been mounted on aerial drones, but with a necessary higher sampling height and, for example, a slung payload to avoid air mixing caused by rotor down-wash (Feitz et al., 2018). These studies, as well as those that perform mobile chemical mapping of

other dynamic surface environments like lakes and rivers (Crawford et al., 2015; Dunbabin and Grinham, 2017; Nicholson et al., 2018), have had to confront technical issues related to sensor stability, sensitivity and response time, anomaly size and magnitude, survey speed, and accurate spatial location, all of which are intrinsically related.

The present paper describes the characteristics and capabilities of the recently developed Ground CO_2 Mapper (or "Mapper" for short), a low-cost, light, robust instrument for sensitive, spatially precise, and rapid mapping of CO_2 concentrations directly at the ground-atmosphere contact. This new prototype greatly improves on the preliminary efforts reported in Jones et al. (2009). Laboratory and field experiments are described which define instrument sensitivity, stability and response time as well as the impact of survey speed, vegetation, and wind conditions on method sensitivity, spatial accuracy and reproducibility. A simple mixing model, which reproduces the experimental data well, is used to estimate Mapper response under leakage rates and survey speeds that were different from those tested. Finally, Mapper and flux surveys conducted at a natural site characterized by extensive geogenic CO_2 leakage are presented to illustrate the tool's sensitivity and reproducibility under real-world conditions.

2. THEORETICAL BACKGROUND

CO_2 leaking from the subsurface can accumulate at the ground-atmosphere interface for two reasons. The first is the higher density of CO_2 (1.8 kg m^{-3}) versus air (1.2 kg m^{-3}), which can lead to stratification (Schwarz et al., 2009; Gasparini et al., 2016). The second is related to wind behavior in the vicinity of the ground surface. Wind speeds display a logarithmic distribution with distance above the ground during neutral atmospheric conditions, with frictional drag induced by surface irregularities and obstacles (such as grass, trees, or buildings) causing wind speeds to reduce to zero within a contact interval known as the roughness height or aerodynamic roughness length (z_0) (Garratt, 1994). This parameter can

be calculated directly using on-site wind profile measurements or inferred using tabulated literature values for different classes of ecosystems or land-use conditions (e.g., Davenport et al. 2000; Montero et al., 2018). Based on the Davenport classification, z_0 values for expected Mapper applications will likely range from 0.5 cm (Class 2: "featureless land surface without any noticeable obstacles and with negligible vegetation") to 3 cm (Class 3: "level country with low vegetation, like grass, and isolated obstacles"). This interval is directly and continuously sampled by the Mapper using a 6mm outer diameter tube dragged on the ground surface (see below).

Although the logarithmic wind profile is strictly true under neutral atmospheric conditions (e.g., a cloudy day with geostrophic winds), it is expected that accumulation will be accentuated under stable conditions and will still occur for variable time periods during more unstable conditions having higher, but intermittent, turbulent mixing.

3. MATERIALS AND METHODS

3.1. The Ground CO_2 Mapper

The basic premise of the Mapper is that a pump continuously draws air from a tube dragged along the ground surface through a small CO_2 NDIR sensor and the measured, geo-referenced concentration is saved to rapidly map ground CO_2 distribution as a proxy of CO_2 leakage flux. While simple in concept, various technical difficulties had to be overcome (e.g., rapid response with low noise) and numerous technological advances were required (e.g., miniaturization, improved batteries, low cost differential GPS, etc.) before it was possible to produce a sensitive, fast-responding, robust, light-weight and low-cost tool (Figure SM-1a).

The sampling tube is a 6 mm outer diameter polypropylene tube with the tip cut at an angle (Figure SM-1b) to lower the risk of drawing soil into the system. This is connected to an in-line, 25 mm diameter, 0.45 μm pore size, cellulose acetate syringe filter followed by a 20 mm diameter micro Non-Dispersive Infrared (NDIR) CO_2 sensor (IRC-A1; Alphasense, Ltd). A

137 hole drilled in the back of the sensor allows direct air flow to a small membrane pump,
138 followed by a second syringe filter just before the outlet that reduces pump-induced pressure
139 pulses.

140 The system contains two ad-hoc electronic boards. The first manages the CO_2 sensor and
141 associated calculations, with the nominal sampling frequency of the IRC-A1 sensor being
142 doubled from 2 to 4 Hz by sampling the leading and following peaks and valleys of the
143 sensor's sinusoidal waveform. The second board integrates a 128 Mb FLASH memory chip
144 for data logging, Wi-Fi connectivity for data downloading, and a low-cost differential GPS
145 antenna that communicates via radio with an associated base station (NEO-M8P; ublox
146 Holding AG) to give up to 10 cm scale accuracy. The entire system is powered by two 18650
147 Li-ion rechargeable batteries (3.7 V, 3400 mAh), which when fully charged give at least 4
148 hours of continual use.

149 The same Mapper unit was used for all measurements, with the only difference being the
150 installation of a more powerful GPS radio antenna after the Ailano surveys and before the test
151 site experiments.

152 **3.2. Other Instruments.**

153 A WindSonic 2-axis ultrasonic anemometer (Gill Instruments, Ltd.), used to monitor wind
154 speed and direction at 4 Hz at a height of 1.5 m during the controlled release experiments,
155 was integrated with a 12V battery / solar panel power supply and a CR300 datalogger
156 (Campbell Scientific, Inc.). This sensor was not available for the surveys at the natural
157 leakage site. An in-house developed flux meter with a 22 cm diameter accumulation chamber
158 was used to conduct point CO_2 flux measurements, with values calculated using the formula
159 reported in Lewicki et al. (2005); previous field comparisons between this and commercial
160 units have yielded equivalent results.

161

3.3. Calculations.

A simple mixing model was created in EXCEL to better understand, and thus predict, Mapper response. It uses the effective flow rate of the pump when mounted in the system (335 cm^3 min^{-1}) and the volume of the sensor chamber (4 cm^3) to mix a known volume of pumped gas with the gas remaining inside the sensor for every 0.05 second time step. This static model was also adjusted to assess system response and sensitivity when the Mapper is in motion. For this, input consists of a profile of 1 cm step intervals, each assigned a ground CO_2 value based on a linear interpolation between bracketing points (i.e., flux measurements transformed to ground surface concentrations using an empirical regression formula) and a time step based on a chosen walking speed. For each 1 cm distance a calculated volume of that interval's concentration is mixed into the sensor volume, with the amount based on the pumping rate and the time step. In some simulations, random sensor noise, based on static monitoring of atmospheric air, is added to each calculated point. To account for the effect of the inlet tube (length = 30 cm; ID = 0.4 cm; volume = 3.96 cm^3), the position of each step is shifted by a fixed amount equal to the time lag (tube volume / pumping rate) times the walking speed. Data is plotted at each 0.25 second interval to mimic the Mapper's 4Hz sampling frequency.

3.4. Test sites

Controlled-release site near Bassano Romano, central Italy. A small-scale experimental site was constructed to test the response and reproducibility of the Mapper system under controlled conditions. It consists of a 2 m long, "L"-shaped leakage plot (1.6 m^2) at the center of a 15 x 25 m field (375 m^2). The field is bounded by bush, a small vineyard, low buildings and sparse trees on its four sides, conditions that may impact wind behavior. The leakage plot (Figures SM-2, SM-3) was built by excavating to a depth of 20 cm, sealing the base and borders with a heavy plastic sheet, covering with 2 cm of sieved soil, distributing perforated 6

187 mm plastic tubing over the entire surface area for gas injection (8 cm tube spacing and 10 cm
188 pin-hole spacing), and then burying the tubes with 5 cm of fine sand, 2 cm of sieved soil, and
189 the original sod to eventually match the surrounding ground level. Tubing connects this plot
190 to a protective cover (Figure SM-3f) that houses a 4 kg canister of food-grade CO_2 (in a hole
191 in the soil to prevent heating) and an inline flowmeter (Figure SM-4). Mapper data were
192 collected at three different walking speeds (ca. 0.6, 2.5, 4.8 km hr^{-1}) along a 16 m long profile
193 that crosses the 2 m long interval of the leakage plot (Figure SM-5), together with CO_2 flux
194 measurements at representative points. Atmospheric air was periodically monitored using the
195 Mapper to define system noise levels and any response changes due to sensor heating; where
196 necessary, the average measured atmospheric value was used to shift other datasets collected
197 at a similar time (typically reducing values by 0-50 ppm). Static Mapper measurements were
198 also conducted for 2-3 minutes at ground surface at points along the profile (in
199 correspondence with flux measurements) to quantify temporal variability. Surveys were
200 performed in June and September, 2020, on sunny days having different wind and CO_2 flux
201 conditions.

202 *Natural CO_2 leakage site near Ailano, southern Italy.* Surveys were conducted in different
203 fields near the town of Ailano, located about 200 km SE of Rome, to test the Mapper under
204 real-world conditions. This area consists of flat to undulating farmland and is known for the
205 wide-spread leakage of geogenic crustal CO_2 (Ascione et al., 2018). Data reported here were
206 collected in October, 2018, from a single, flat, 4600 m^2 field with <2 cm tall vegetation
207 (Figure SM-6); in contrast to the experimental site, this field is surrounded on all four sides
208 by open cultivated fields with similar low vegetation. CO_2 leakage occurs from a number of
209 variably sized "hot-spot" areas, with measured flux rates as high as 2000 g m^{-2} d^{-1} but with
210 most leakage areas well below 800 g m^{-2} d^{-1}. At the time of the survey the visible impact of
211 the CO_2 leakage on vegetation was weak (Figure SM-6), limited primarily to thinner grass in

212 the areas of strongest flux. Mapper surveys were conducted by walking a series of parallel
213 lines spaced 2-4 m apart at speeds of ca. 2.5 or 5.0 km hr^{-1}. Flux measurements were
214 performed on a regular 10m spacing grid (60 points), with an additional 20 points collected
215 between grid points to better define observed anomalies.

216 **4. RESULTS AND DISCUSSION**

217 **4.1. Laboratory tests and modelling**

218 System noise was assessed by first warming up the sensor for 30 minutes, followed by
219 pumping a 400 ppm CO_2 standard for another 30 minutes and monitoring the response. This
220 laboratory test yielded $2\sigma = 16$ ppm (Figure 1a), while similar results were always obtained
221 for periodic, shorter duration monitoring of atmospheric air conducted during the controlled
222 release experiments.

223 Continuous peak and valley sampling of the NDIR waveform, conducted to increase the
224 sampling frequency to 4 Hz for higher spatial resolution, introduces a different type of noise
225 when the sensor is exposed to a very rapid concentration change (Figure 1b). This "saw-
226 tooth" trend is very regular, and thus a simple 2-point running average provides a smooth and
227 accurate representation. This averaging improves anomaly definition for surveys along
228 profiles and further reduces system noise (e.g., $2\sigma = 14$ ppm for the dataset above).

229 Reproducibility of the system was tested by alternating between pure nitrogen and a 400
230 ppm CO_2 standard for approximately ten seconds each (Figure 1c). Overlaying the five 0 to
231 400 ppm cycles shows excellent reproducibility (Figure 1d), both in terms of response time
232 and absolute concentrations at the two extremes. Based on these results, system response time
233 is defined as $T_{67} = 0.75$ seconds and $T_{90} = 1.55$ seconds (i.e., the time required to reach 67%
234 and 90%, respectively, of the new value). The strong similarity between the lab and
235 associated modelling results (Figure 1d) indicates that this response is controlled by simple
236 mixing in the sensor.

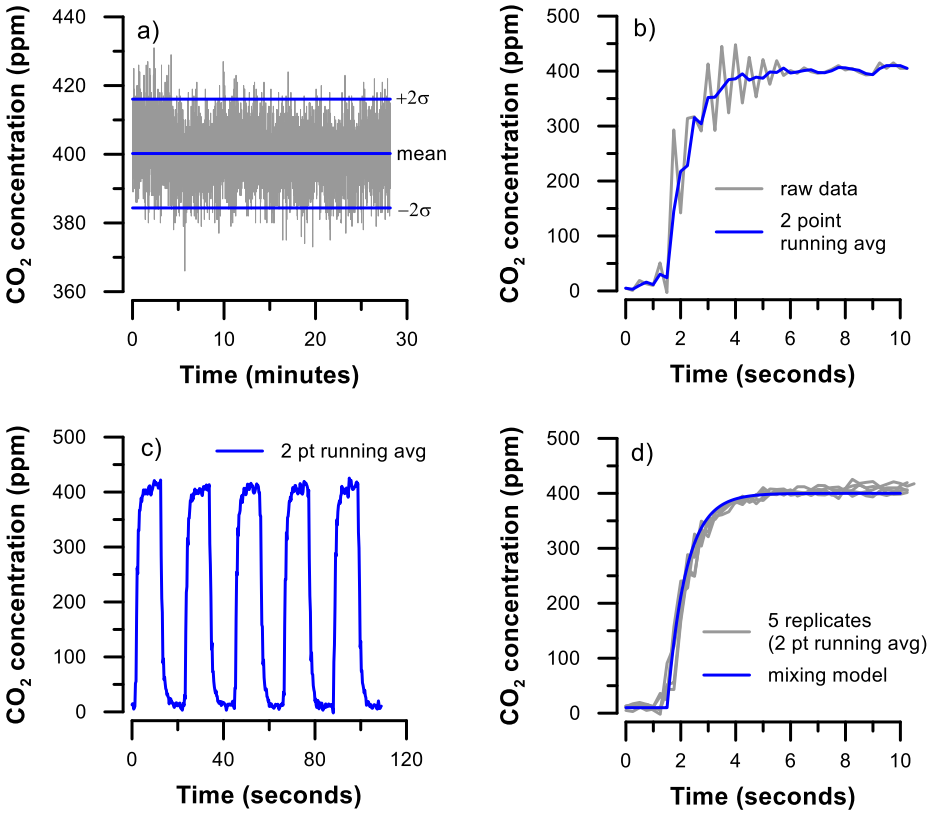

Figure 1. Laboratory data illustrating the Mapper response characteristics, including: (a) system noise; (b) saw-tooth trend during a rapid concentration change; (c) response time and reproducibility; and (d) modelling of the system response relative to the data in (c).

Note that a compromise had to be found between response time and noise during development, as these tend to be inversely related (i.e., increased pump flow decreases the former but the associated greater turbulence and pressure fluctuations increases the latter). As discussed below, a fast response time is critical for a mobile platform, both in terms of accurately locating and delineating anomalies as well as overall sensitivity.

4.2. Controlled release test site

To illustrate the importance of sampling height, the Mapper sampling tube was fixed at 0, 5 and 20 cm above the CO_2 injection plot (at a point having a measured CO_2 flux of 190 g m^{-2} d^{-1}) and left to monitor for approximately 4 minutes each (Figure 2a). The range of values measured at ground surface, within the 2-3 cm tall grass, greatly exceed those observed just

above the grass at 5 cm height, while those at 20 cm height are similar to monitoring of atmospheric air. These results demonstrate how CO_2 accumulation within the friction height can yield significant anomalies above a CO_2 leakage area (thus making it a valid sampling target for a mobile measurement platform) compared to the much greater dilution observed at only a few centimeters above the ground surface.

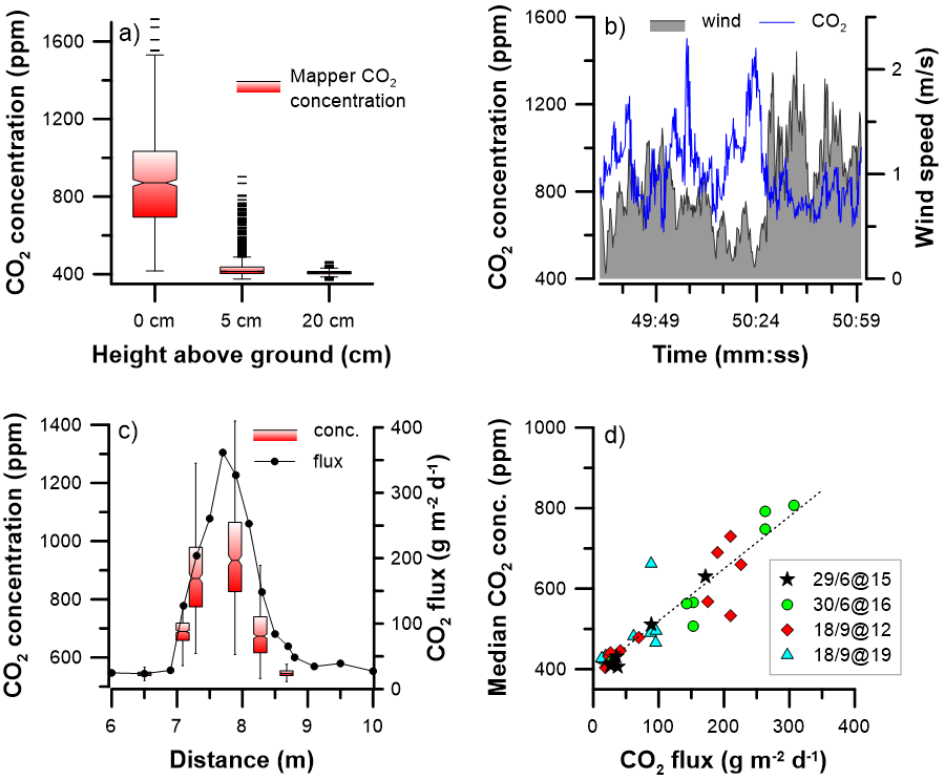

Figure 2. Plots showing Mapper response during static tests at the controlled release site: (a) fixed monitoring at different heights above a point with 190 g m^{-2} d^{-1} CO_2 flux; (b) example of impact of wind strength on ground CO_2 concentration; (c) range of ground CO_2 concentrations (without outliers) during 2-3 minute monitoring periods together with CO_2 flux at various points across the leakage plot on 30/6/20; and (d) comparison of CO_2 flux and median ground CO_2 values for the data in (c) and other similar tests (day/month@hour).

The ground surface measurements in Figure 2a (i.e., 0 cm) are also striking for the wide range of values observed, from a minimum near atmospheric levels to a maximum of 1700 ppm CO_2 and an inter-quartile range from 700 to 1000 ppm CO_2. This shows how the

266 measured parameter can be highly dynamic, controlled primarily by wind strength variations
267 (Figure 2b). Although this indicates that Mapper surveys should probably not be conducted
268 on very windy days, two points should be highlighted. First, a leakage area will be sampled
269 continuously as it is traversed, meaning that oscillating wind strength and / or minor changes
270 in vegetation density while moving across an anomaly could still result in a portion being
271 sampled that has greater CO_2 accumulation. Because of this variability, sensitivity can also be
272 assessed in terms of probability, as is discussed below. Second, the method's speed means
273 that multiple, repeat surveys can be rapidly conducted to reduce wind-induced uncertainty.
274 Although CO_2 concentrations within the friction height can be variable, CO_2 flux and
275 ground CO_2 concentration ranges measured at the same points show a similar trend along the
276 profile (Figure 2c). Plotting flux values against median ground CO_2 concentrations for this
277 dataset and similar tests performed on different days (Figure 2d) defines a clear linear
278 correlation between these two variables:

279 $$[CO_2] = 1.3 \times CO_2 \text{ flux} + 391; (R^2 = 0.88) \qquad \text{Eqn. 1}$$

280 Based on this regression formula, a 50 g m^{-2} d^{-1} flux anomaly should yield a median ground
281 CO_2 concentration of 456 ppm compared to a value of 417 ppm for a background flux of 20 g
282 m^{-2} d^{-1} (for these site / survey conditions). The difference of 39 ppm between these two is
283 more than double the noise level of the Mapper (2σ=16 ppm), indicating that the system may
284 be able to recognize such a low-level anomaly. However, this does not take into consideration
285 the actual response of the system when in movement and impacted by the combined effects
286 of survey speed, anomaly size and response time, or the spatial variability of the background
287 biological CO_2 flux field. The former is examined in more detail below, while the latter is
288 highly site specific and dependent on survey conditions (e.g., dry periods may yield a lower,
289 more uniform background flux).

The response and reproducibility of the Mapper while in movement was tested on 17/9/20 by measuring the 16 m long profile 10 times for each of three walking speeds (ca. 0.6, 2.5, 4.8 km hr^{-1}); this was repeated during three different time periods (12:30-13:15; 16:00-16:40; 17:00-17:40) for a total of 30 profiles per speed. Winds were light (average of 3.5 km hr^{-1} with gusts up to 10 km hr^{-1}), relatively similar during the three periods (Figure 3a), and primarily from the NW quadrant (Figure 3b). The CO_2 injection rate from the canister was 30 ml min^{-1}, which resulted in a 1.7 m long, asymmetrical interval of anomalous CO_2 leakage along the profile (7.3-9 m) with a maximum flux rate of 260 g m^{-2} d^{-1} at 8.8 m (e.g., Figure 3e).

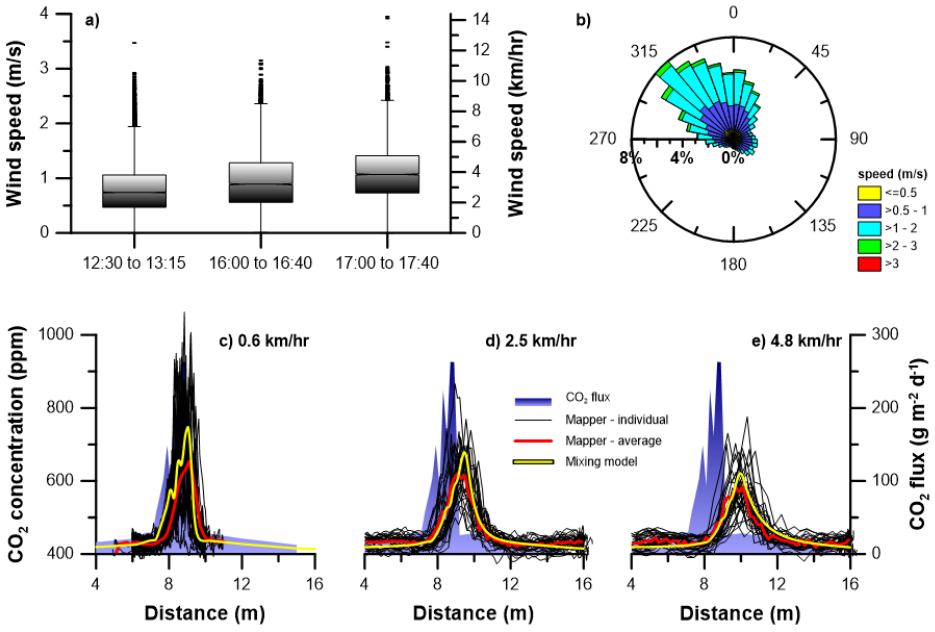

Figure 3. Data from reproducibility tests at the Bassano controlled release site on 17/9/20: a) wind speed distribution during the three measurement periods; b) wind direction during all test periods; c) – e) 30 Mapper replicates (2-point running average) and associated total average for three different survey speeds, together with modelled Mapper response based on the median ground CO_2 concentrations calculated using the shown flux distribution and Eqn. 1.

306 Plots of all 30 replicates for each of the three walking speeds show good reproducibility for
307 both peak location (despite the inherent GPS uncertainty) and anomaly magnitude (Figure
308 3c,d,e; Table 1) over the 5 hour time span of the surveys. The average trace for each plot (red
309 line) illustrates how survey speed impacts the Mapper response, with the anomaly peak
310 becoming lower, wider, and more offset with increasing walking speeds (Table 1). That said,
311 all 30 profiles at the fastest walking speed of 4.8 km hr^{-1} registered the anomaly, gave an
312 average offset of only 1.2 m, and the smallest of these peaks (i.e., 91 ppm above background)
313 was still > 5 times higher than the 2σ noise level of the instrument (16 ppm).
314
315 Table 1. Summary statistics for the Mapper profiles conducted on 17/09/20 at the Bassano
316 controlled release site (see Figure 3); note that peak height refers to measured maximum
317 value minus background. Thirty replicates were performed for each of the three walking
318 speeds.

	Peak location (m)			***Peak width (m)***			***Peak height (ppm)***		
walking speed (km hr^{-1})	**0.6**	**2.5**	**4.8**	**0.6**	**2.5**	**4.8**	**0.6**	**2.5**	**4.8**
minimum	8.3	8.5	9.2	1.1	2.1	2.3	89	84	91
maximum	9.6	10.2	10.8	3.1	4.4	5.3	618	432	320
average	8.9	9.3	10.0	2.0	3.0	3.5	397	234	176
standard deviation (1σ)	0.3	0.4	0.4	0.4	0.6	0.7	121	65	61

319
320 The mobile Mapper response was also assessed by comparing the data collected on 17/9/20
321 with results from the dynamic mixing model. Model input conditions were defined by
322 converting the 18 flux measurements reported in Figure 3 into median ground CO_2
323 concentrations using Eqn. 1, with sensor noise excluded. The good match in Figure 3c-e
324 between the average Mapper response (red lines) and the dynamic mixing model (yellow
325 lines) for the different walking speeds show that the controlling mechanisms are well
326 understood and that the model can used to predict response under other conditions (see
327 below).

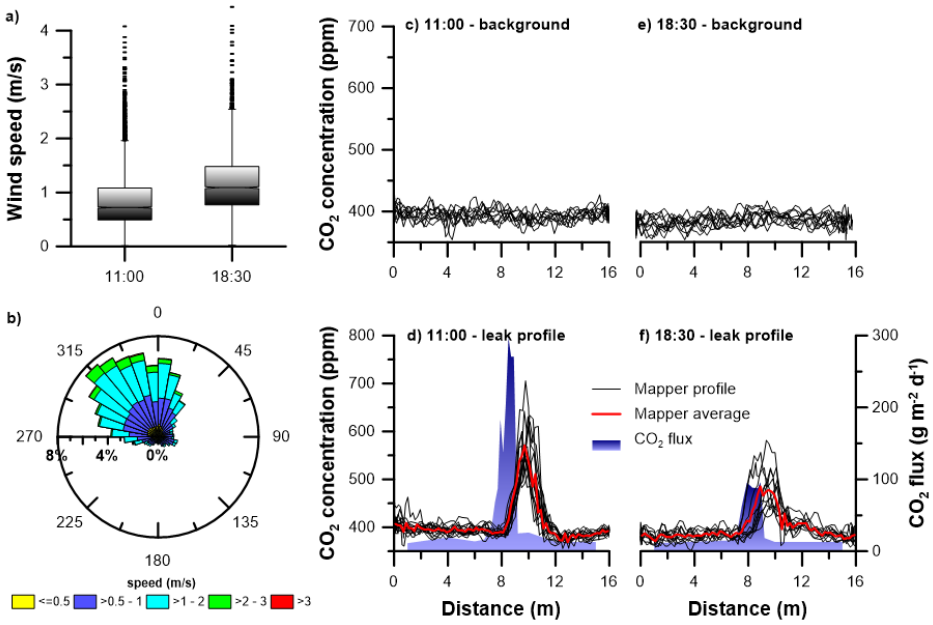

328

329 **Figure 4.** Data from sensitivity tests at the Bassano controlled release site on 18/9/20: a)
330 wind speed distribution during the two measurement periods; b) wind direction during both
331 periods; Mapper profiles outside (c, e) and across (d, f) the leakage plot at around 11:00 and
332 18:30, respectively. Note all profiles were performed at a survey speed of about 2.5 km hr^{-1}.

333 The subsequent morning (18/9/20) the CO_2 flux and ground concentrations were measured,
334 the gas injection stopped, and then the measurements were repeated about 8 hours later after
335 the flux rate had reduced; note that all Mapper surveys were performed at 2.5 km hr^{-1}. Wind
336 conditions during both measurement periods (Figure 4a, b) were similar to those of the
337 previous day (Figure 3a, b). Mapper profiles conducted parallel to, but only 50 cm outside the
338 injection pit during both periods (Figure 4c, e) yielded consistently low values with noise
339 levels (2σ= 22 ppm) only slightly higher than those for atmospheric air monitoring (2σ= 16
340 ppm), indicating no lateral smearing of the ground CO_2 anomaly. Early morning Mapper
341 surveys across the leak (Figure 4d), prior to stopping gas injection, yielded results similar to
342 those observed the previous day (Figure 3d), both for the maximum flux rate (ca. 250 g m^{-2} d^{-1})
343 and the peak value of the average Mapper response (575 ppm). Eight hours after the gas
344 had been turned off the flux anomaly was still about 1.5 m wide but was truncated at a

345 relatively constant value of about 90 g m^{-2} d^{-1} across a 1 m interval (Figure 4f). Even at this
346 much lower flux rate the Mapper profiles clearly define the anomaly, with 10 replicates
347 resulting in an average maximum peak height of about 75 ppm above background (red line in
348 Figure 4f).

349 To further examine the Mapper's lower detection limit, below that tested in the previous
350 experiment, dynamic mixing modelling was performed using three synthetic, 2 m wide,
351 symmetrical CO_2 leakage anomalies having a maximum central flux rate of 100, 75, and 50 g
352 m^{-2} d^{-1} (Figure 5) in a background flux field of 20 g m^{-2} d^{-1}. Each of the three synthetic flux
353 distributions were first converted into equivalent ground CO_2 concentrations for model input.
354 Considering, however, that ground concentrations can change due to wind fluctuations
355 (Figure 2b), multiple flux-to-concentration regression equations like Eqn. 1 were created
356 across the entire range of observed conditions (assuming that the highest winds result in the
357 lowest ground CO_2 concentrations at all points, and vice versa).

358 To accomplish this, the first 2 minutes of data (4 Hz x 120 seconds = 480 points) from all
359 35 fixed-point Mapper monitoring tests discussed above were individually ordered from
360 lowest to highest in sequential columns of a spread sheet, with the associated measured flux
361 value in the first row. Regression formulas were then calculated for CO_2 flux versus each 10^{th}
362 percentile of ground concentration values (i.e., line 1 versus line 2, line 49, line 97, etc.).
363 These formulas ranged from $[CO_2]$ = 0.51 x CO_2 flux + 391 for the lowest CO_2
364 concentrations measured for each flux rate to $[CO_2]$ = 3.36 x CO_2 flux + 401 for the highest,
365 with R^2 values from 0.67 to 0.88, respectively. These 10 equations were used to convert each
366 of the three synthetic flux distributions into 10 different ground CO_2 concentration
367 distributions for model input, and then the Mapper response (with system noise) was
368 simulated for each at survey speeds of 2.5 and 4.8 km hr^{-1}. Figure 5 shows these simulated
369 Mapper results as grey lines, except for one in black which represents the first simulation that

370 clearly defines the anomaly (i.e., the lowest percentile of input ground CO_2 concentration that
371 yields a Mapper anomaly that is more than twice the 2σ noise level and wider than the noise
372 frequency). To facilitate comparison, some simulation datasets were shifted downwards
373 slightly (typically < 25 ppm) to standardize the background response at ca. 400 ppm.

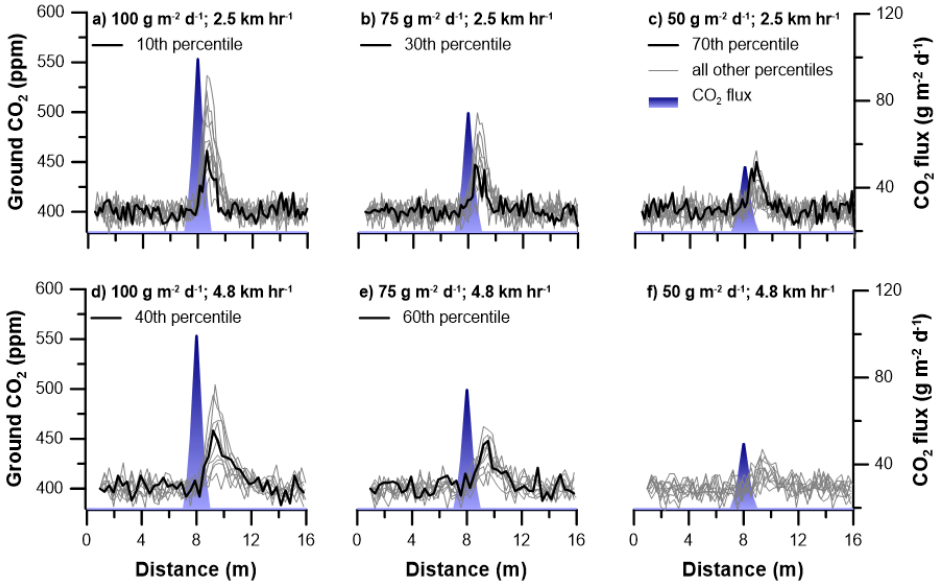

374

375 **Figure 5.** Simulations of the Mapper response while traversing a synthetic, 2 m-wide,
376 symmetrically distributed leakage area, taking into consideration system noise. Two different
377 survey speeds and three different maximum flux rates are shown (see legends). Grey lines
378 represent Mapper simulation results while the thick black lines highlight the "first"
379 simulation (i.e., lowest input percentile) that clearly defines the anomaly (see text for details).

380 As expected, the probability of recognizing an anomaly decreases with decreasing flux and
381 increasing survey speed. For example, Figure 5a shows how 90% of the 2.5 km hr^{-1} surveys
382 (i.e., the 10^{th} percentile and upwards) clearly define the 100 g m^{-2} d^{-1} flux anomaly, compared
383 to 70% (Figure 5b) and 30% (Figure 5c) that clearly find the 75 and 50 g m^{-2} d^{-1} anomalies,
384 respectively. Instead, for the faster survey speed of 4.8 km hr^{-1}, the 100 and 75 g m^{-2} d^{-1}
385 anomalies are recognised by 60% (Figure 5d) and 40% (Figure 5e) of the simulated surveys,
386 whereas there is little probability that the Mapper can clearly define the 50 g m^{-2} d^{-1} anomaly

387 at this survey speed (Figure 5f). Based on a probability of success greater than 60%, the
388 estimated detection limit for the Mapper (when it crosses an anomaly) is 75 g m^{-2} d^{-1} at a 2.5
389 km hr^{-1} survey speed and 100 g m^{-2} d^{-1} at a 4.8 km hr^{-1} survey speed, under these site
390 conditions.

391 The controlled field experiments also highlighted some limitations of the ground CO_2
392 method which should be taken into consideration when planning and conducting Mapper
393 surveys. First, very high quality positioning data is critical for producing useful data, and thus
394 the GPS base station must always be within a reasonable distance (e.g., <100 m) and have a
395 clear line of site with the mobile unit. For this reason, forested areas would be very difficult
396 to survey. Second, site conditions must be considered to safeguard the instrument and
397 produce high quality data. For example: i) surveying with wet ground conditions (including
398 morning dew) risks blocking the filter or damaging the sensor; ii) long grass may favor CO_2
399 accumulation but it is difficult to maintain the sampling tube at ground level; and iii) highly
400 variable vegetation conditions (density, height) can result in a more variable baseline. Third,
401 the area being surveyed should be free of shadows when working on very hot sunny days
402 with little wind, as shaded areas have lower heat-induced convection and thus biological CO_2
403 can accumulate and produce anomalies that are unrelated to leakage.

404 **4.3. Natural CO_2-leakage site**

405 Flux in the 4600 m^2 field near Ailano was initially measured at 60 points on a regular ca.
406 10 m grid (Figure 6a), followed by an additional 20 in-fill samples to better define spatial
407 distribution (Figure 6b). Despite the very high sampling density of the former (13,000
408 samples km^{-2}), it still misses or poorly defines various leakage areas compared to the latter
409 (17,000 samples km^{-2}).

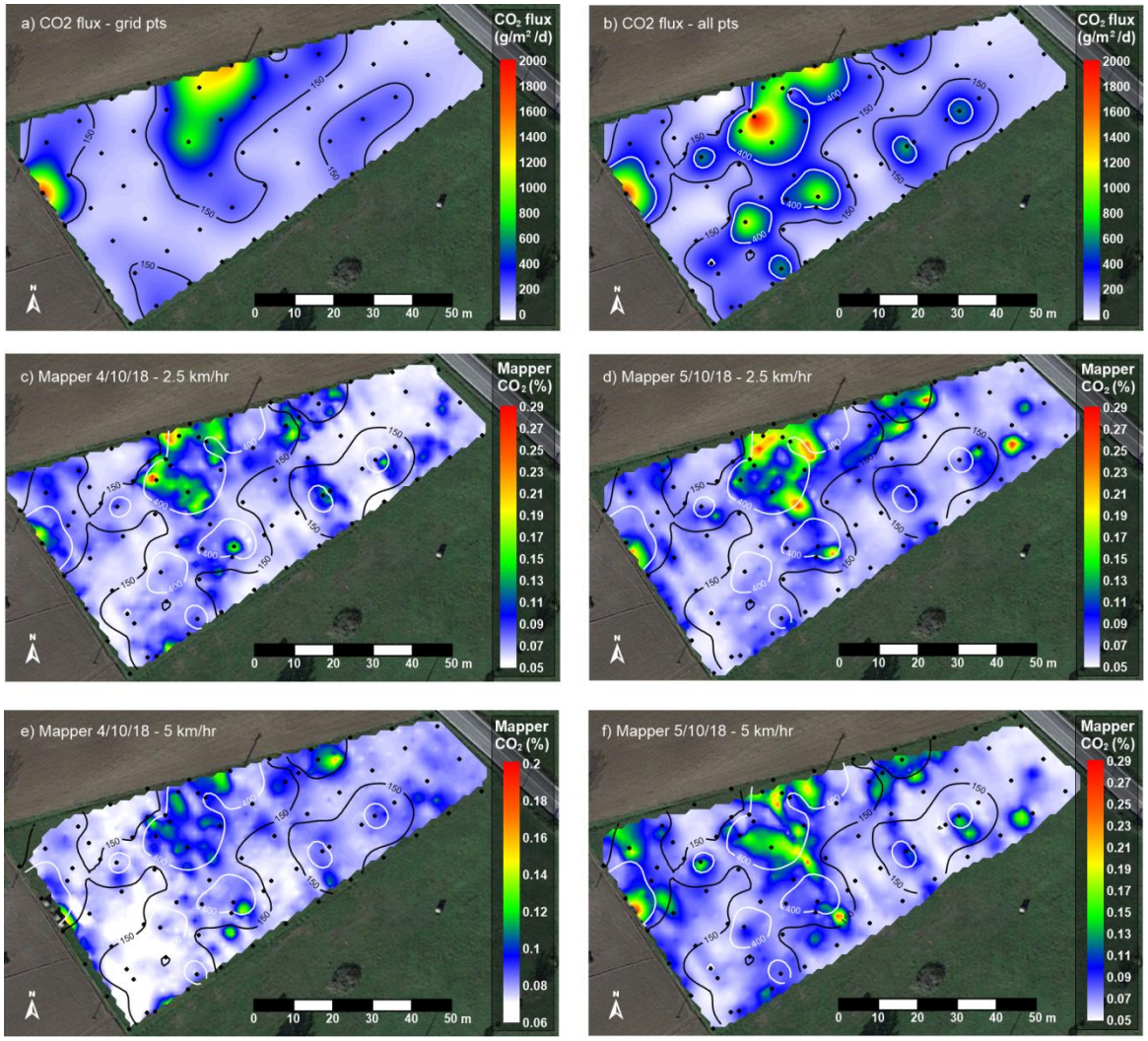

410

411 **Figure 6.** Field data from a site near Ailano, Italy: (a) CO_2 flux measured on a regular 10 m
412 grid and (b) with additional in-fill points; Mapper surveys conducted at 2.5 km hr^{-1} on
413 4/10/18 (c) and 5/10/18 (d) and at 5 km hr^{-1} on 4/10/18 (e) and 5/10/18 (f). The flux
414 measurement points (black dots) and the 150 and 400 g m^{-2} d^{-1} flux contours from (b) are
415 plotted on the Mapper results for spatial reference. Mapper measurement points are excluded
416 to improve clarity but are given in Figure SM-7.

417 The field was subsequently surveyed with the Mapper at different speeds during two sunny
418 days that had light winds averaging around 1 km hr^{-1}. Surveys performed at 2.5 km hr^{-1} on
419 4/10/18 (Figure 6c) and 5/10/18 (Figure 6d) show very similar distributions and magnitudes.
420 Both locate most of the main flux anomalies observed in Figure 6b, define them in a much

more spatially restricted manner, and outline additional leakage spots that were missed by the point flux measurements. Even at twice the walking speed, the two surveys conducted at 5 km hr^{-1} on 4/10/18 (Figure 6e) and 5/10/18 (Figure 6f) show comparable results. Neither survey speed appears to produce significant anomaly smearing, despite maximum flux rates that are approximately 10 times higher than those used during the controlled release experiments.

Aside from the main gas leakage anomalies described above it should also be pointed out that lower-level diffuse leakage occurs throughout much of this field, with only 9 measurement points (11%) having CO_2 flux values less than 24 g m^{-2} d^{-1} while all others appear to be part of a single, leakage-related population (Figure 7a). Similarly, the Mapper results from 4/10/18 at a walking speed of 2.5 km hr^{-1} only show a very limited number of points in the baseline range (Figure 7b), which is estimated to be around 550 ppm on this day as a function of sensor calibration and temperature (unfortunately, atmospheric monitoring with the Mapper was not conducted). This plot, with its numerous smaller peaks, highlights the capability of the Mapper to define not only strong spot leaks but also lower-level diffuse leakage. This is also illustrated by contouring one of the Mapper datasets (Figure 6c) on a log scale (Figure 7c).

Finally, it is important to note that the flux survey took about 300 minutes to complete (based on an average measurement time of ca. 3 minutes per point plus the time to lay out the grid), whereas the Mapper surveys at 2.5 and 5 km hr^{-1} only took about 30-40 and 15-20 minutes, respectively. Despite requiring only 5-10% of the time, the resultant ground CO_2 maps highlight a far-more complex gas leakage distribution than would be logistically possible to define with point flux measurements.

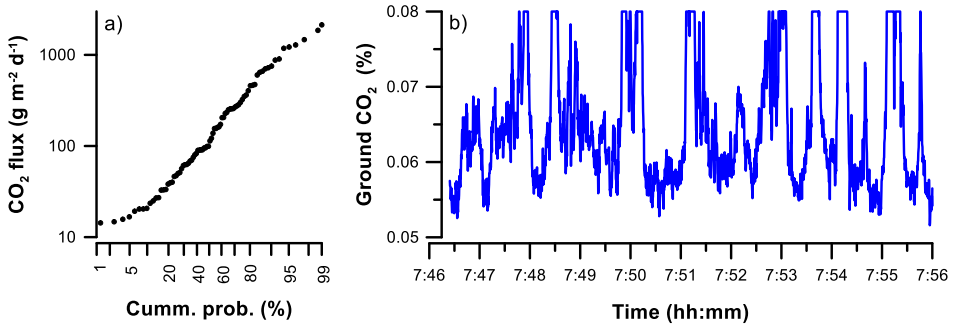

444

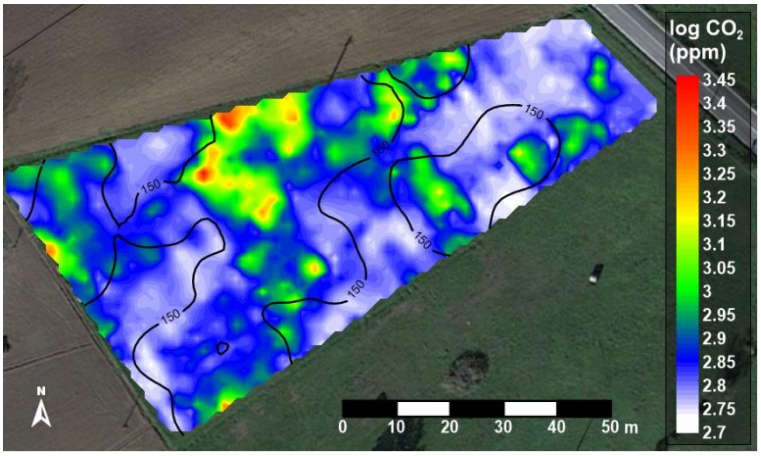

445

446 **Figure 7.** Additional plots of the Ailano field data: (a) cumulative probability plot of the flux
447 dataset; (b) representative 10 minutes of the Mapper data from the NE end of Figure 6c,
448 plotted with a 2 point running average and truncated at 800 ppm to highlight lower
449 concentration trends; and (c) same as Figure 6c but plotted as a logarithmic scale of ppm
450 values (150 g m^{-2} d^{-1} CO_2 flux contour from Figure 6b given for spatial reference).

451 ## 5. Conclusions

452 The results detailed above define the characteristics and capabilities of the newly developed
453 Ground CO_2 Mapper under real-world conditions, illustrating its potential for improving
454 point flux surveys focused on finding and/or quantifying the leakage of deep-origin CO_2 from
455 the ground surface to the atmosphere. In particular, this low-cost, robust, and easy-to-use tool
456 is sensitive, yields spatially detailed and reproducible results, and is very rapid.

457 It is foreseen that the Mapper will complement traditional point flux surveys, providing a
458 secondary dataset that will improve overall results in numerous ways. For example, initial

Mapper results can help define appropriate flux measurement locations and densities, be it a uniform grid spacing or variable densities that focus data collection on areas of greater spatial variability. This can reduce the time necessary to conduct a field campaign, thus decreasing overall costs or freeing resources for other work (e.g., soil gas analyses to better separate leakage from background populations). Because it is so rapid, reconnaissance surveys can be conducted to better link CO_2 leakage to regional features (like faults or lithological boundaries) in diffuse degassing studies or to find small leaks during CCS monitoring, and multiple surveys can be performed to reduce uncertainties.

To further develop this tool, future work will focus on improving its response (lower noise, faster response), robustness, and ease of use. In addition, testing is underway to understand if the qualitative, high density ground CO_2 concentration data provided by the Mapper can be combined with point flux survey results, via multivariate geostatistical methods like co-kriging and kriging with external drift, to reduce uncertainties in total leakage flux estimates

CRediT authorship contribution statement

Stefano Graziani: Conceptualization, Methodology, Software, Investigation, Writing - Original Draft; **Stan E. Beaubien**: Conceptualization, Validation, Investigation, Writing - Review & Editing; **Giancarlo Ciotoli**: Formal analysis, Data Curation, Writing - Review & Editing; **Sabina Bigi**: Supervision, Project Administration, Funding Acquisition, Writing - Review & Editing.

Data Availability

Datasets related to this article can be found at …

Declaration of competing interest

The authors declare that they have no known competing financial interests or personal relationships that could have appeared to influence the work reported in this paper.

Acknowledgments

This research has received funding from the European Union's Horizon 2020 Research and Innovation Programme under Grant Agreement No 653718 (ENOS – Enabling Onshore CO_2 Storage in Europe). The construction and use of the Bassano Romano test site was possible due to the kind generosity of the land owner Luigi Meloni. Maria Chiara Tartarello is gratefully acknowledged for her assistance in collecting the Ailano field data.

Appendix A. Supplementary material and data.

Supplementary material to this article, including photographs and additional plots, can be found online at …

Supplementary data to this article can be found online at …

References

Annunziatellis, A., Beaubien, S.E., Bigi, S., Ciotoli, G., Coltella, M. and Lombardi, S., 2008. Gas migration along fault systems and through the vadose zone in the Latera caldera (central Italy): Implications for CO_2 geological storage. Int. J. Greenhouse Gas Control, 2/3: 353-372. DOI:10.1016/j.ijggc.2008.02.003

505 Annunziatellis, A., Beaubien, S.E., Ciotoli, G., Coltella, M. and Lombardi, S., 2008.
506 Development of a rapid, low-cost technique for sensitive CO_2 leakage mapping, Vol. 10,
507 EGU2008-A-10641, EGU General Assembly 2008, Vienna, Austria.

508 Ascione, A., Ciotoli, G., Bigi, S., Buscher, J., Mazzoli, S., Ruggiero, L., Sciarra, A.,
509 Tartarello, M.C. and Valente, E., 2018. Assessing mantle versus crustal sources for non-
510 volcanic degassing along fault zones in the actively extending southern Apennines mountain
511 belt (Italy). GSA Bulletin, 130(9-10): 1697-1722. DOI:10.1130/b31869.1

512 Barkwith, A.K.A.P., Beaubien, S.E., Barlow, T., Kirk, K., Lister, T.R., Tartarello, M.C. and
513 Taylor, H., 2020. Using near-surface atmospheric measurements as a proxy for quantifying
514 field-scale soil gas flux. Geoscience Instrumentation, Methods and Data Systems.
515 DOI:10.5194/gi-2020-8

516 Barron-Gafford, G.A., Scott, R.L., Jenerette, G.D. and Huxman, T.E., 2011. The relative
517 controls of temperature, soil moisture, and plant functional group on soil CO_2 efflux at diel,
518 seasonal, and annual scales. Journal of Geophysical Research: Biogeosciences, 116(G1).
519 DOI:10.1029/2010JG001442

520 Beaubien, S.E., Ciotoli, G., Finoia, M.G., Lombardi, S. and Bigi, S., 2022. Monte Carlo
521 simulations to assess the uncertainty of locating and quantifying CO_2 leakage flux from deep
522 geological or anthropogenic sources. Stochastic Environmental Research and Risk
523 Assessment. DOI:10.1007/s00477-021-02123-9

524 Bigi, S., Beaubien, S.E., Ciotoli, G., D'Ambrogi, C., Doglioni, C., Ferrante, V., Lombardi,
525 S., Milli, S., Orlando, L., Ruggiero, L., Tartarello, M.C. and Sacco, P., 2014. Mantle-derived
526 CO_2 migration along active faults within an extensional basin margin (Fiumicino, Rome,
527 Italy). Tectonophysics, 637(0): 137-149. DOI:10.1016/j.tecto.2014.10.001

528 Cardellini, C., Chiodini, G. and Frondini, F., 2003. Application of stochastic simulation to
529 CO_2 flux from soil: Mapping and quantification of gas release. Journal of Geophysical
530 Research: Solid Earth, 108(B9): 2425. DOI:10.1029/2002JB002165

531 Chiodini, G., Cardellini, C., Amato, A., Boschi, E., Carliro, S. and Frondini, F., 2004.
532 Carbon dioxide Earth degassing and seismogenesis in central and southern Italy. Geophysical
533 Research Letters, L07615: doi:10.1029/2004GL019480.

534 Chiodini, G., Cardellini, C., Bini, G., Frondini, F., Caliro, S., Ricci, L. and Lucidi, B., 2021.
535 The Carbon Dioxide Emission as Indicator of the Geothermal Heat Flow: Review of Local
536 and Regional Applications with a Special Focus on Italy. Energies, 14(20): 6590.

537 Crawford, J.T., Loken, L.C., Casson, N.J., Smith, C., Stone, A.G. and Winslow, L.A., 2015.
538 High-Speed Limnology: Using Advanced Sensors to Investigate Spatial Variability in
539 Biogeochemistry and Hydrology. Environmental Science & Technology, 49(1): 442-450.

540 Davenport, A.G., Grimmond, C., Oke, T. and Wieringa, J., 2000. Estimating the roughness
541 of cities and sheltered country, 15th conference on probability and statistics in the
542 atmospheric sciences / 12th conference on applied climatology. American Meteorological
543 Society, Ashville, NC, USA, pp. 96-99.

544 Dunbabin, M. and Grinham, A., 2017. Quantifying Spatiotemporal Greenhouse Gas
545 Emissions Using Autonomous Surface Vehicles. Journal of Field Robotics, 34(1): 151-169.

546 Elío, J., Ortega, M.F., Nisi, B., Mazadiego, L.F., Vaselli, O., Caballero, J. and Chacón, E.,
547 2016. A multi-statistical approach for estimating the total output of CO_2 from diffuse soil
548 degassing by the accumulation chamber method. Int J Greenhouse Gas Control, 47: 351-363.
549 DOI:10.1016/j.ijggc.2016.02.012

550 Feitz, A., Schroder, I., Phillips, F., Coates, T., Negandhi, K., Day, S., Luhar, A., Bhatia, S.,
551 Edwards, G., Hrabar, S., Hernandez, E., Wood, B., Naylor, T., Kennedy, M., Hamilton, M.,
552 Hatch, M., Malos, J., Kochanek, M., Reid, P., Wilson, J., Deutscher, N., Zegelin, S., Vincent,
553 R., White, S., Ong, C., George, S., Maas, P., Towner, S., Wokker, N. and Griffith, D., 2018.
554 The Ginninderra CH4 and CO_2 release experiment: An evaluation of gas detection and
555 quantification techniques. International Journal of Greenhouse Gas Control, 70: 202-224.

556 Gal, F., Pokryszka, Z., Labat, N., Michel, K., Lafortune, S. and Marblé, A., 2019. Soil-Gas
557 Concentrations and Flux Monitoring at the Lacq-Rousse CO_2-Geological Storage Pilot Site
558 (French Pyrenean Foreland): From Pre-Injection to Post-Injection. Applied Sciences, 9(4):
559 645.

560 Garratt, J.R., 1994. Review: the atmospheric boundary layer. Earth-Science Reviews,
561 37(1): 89-134.

562 Gasparini, A., Sainz-García, A., Grandia, F. and Bruno, J., 2016. Atmospheric dispersion
563 modelling of a natural CO_2 degassing pool from Campo de Calatrava (northeast Spain)
564 natural analogue. Implications for carbon storage risk assessment. International Journal of
565 Greenhouse Gas Control, 47: 38-47.

566 Jenkins, C., 2020. The State of the Art in Monitoring and Verification: an update five years
567 on. International Journal of Greenhouse Gas Control, 100: 103118.

568 Jones, D.G., Barkwith, A.K.A.P., Hannis, S., Lister, T.R., Gal, F., Graziani, S., Beaubien,
569 S.E. and Widory, D., 2014. Monitoring of near surface gas seepage from a shallow injection
570 experiment at the CO_2 Field Lab, Norway. International Journal of Greenhouse Gas Control,
571 28: 300-317.

572 Jones, D.G., Barlow, T., Beaubien, S.E., Ciotoli, G., Lister, T.R., Lombardi, S., May, F.,
573 Moller, I., Pearce, J.M. and Shaw, R.A., 2009. New and established techniques for surface
574 gas monitoring at onshore CO_2 storage sites. Energy Procedia, 1(1): 2127-2134.

575 Krevor, S., Perrin, J.-C., Esposito, A., Rella, C. and Benson, S., 2010. Rapid detection and
576 characterization of surface CO_2 leakage through the real-time measurement of $\delta^{13}C$
577 signatures in CO_2 flux from the ground. International Journal of Greenhouse Gas Control,
578 4(5): 811-815.

579 Kutzbach, L., Schneider, J., Sachs, T., Giebels, M., Nykänen, H., Shurpali, N.J.,
580 Martikainen, P.J., Alm, J. and Wilmking, M., 2007. CO_2 flux determination by closed-
581 chamber methods can be seriously biased by inappropriate application of linear regression.
582 Biogeosciences, 4(6): 1005-1025.

583 Lewicki, J.L., Bergfeld, D., Cardellini, C., Chiodini, G., Granieri, D., Varley, N. and
584 Werner, C., 2005. Comparative soil CO_2 flux measurements and geostatistical estimation
585 methods on Masaya volcano, Nicaragua. Bull Volcanol, 68: 76-90. DOI:10.1007/s00445-
586 005-0423-9

587 Montero, G., Rodríguez, E. and Oliver, A., 2018. Characterization of Geographical and
588 Meteorological Parameters. In: R. Perez (Editor), Wind Field and Solar Radiation
589 Characterization and Forecasting: A Numerical Approach for Complex Terrain. Springer
590 International Publishing, Cham, pp. 41-63. DOI:10.1007/978-3-319-76876-2_2

591 Nicholson, D.P., Michel, A.P.M., Wankel, S.D., Manganini, K., Sugrue, R.A., Sandwith,
592 Z.O. and Monk, S.A., 2018. Rapid Mapping of Dissolved Methane and Carbon Dioxide in
593 Coastal Ecosystems Using the ChemYak Autonomous Surface Vehicle. Environmental
594 Science & Technology, 52(22): 13314-13324.

595 Oertel, C., Matschullat, J., Zurba, K., Zimmermann, F. and Erasmi, S., 2016. Greenhouse
596 gas emissions from soils - A review. Geochemistry, 76(3): 327-352.

597 Oldenburg, C., Lewicki, J., Pan, L., Dobeck, L. and Spangler, L., 2010. Origin of the
598 patchy emission pattern at the ZERT CO_2 release test. Environmental Earth Sciences, 60(2):
599 241-250.

600 Oldenburg, C.M. and Unger, A.J.A., 2004. Coupled vadose zone and atmospheric surface
601 layer transport of carbon dioxide from geologic carbon sequestration sites. Vadose Zone
602 Journal, 3: 848-857.

603 Roberts, J.J., Wood, R.A., Wilkinson, M. and Haszeldine, S., 2015. Surface controls on the
604 characteristics of natural CO_2 seeps: implications for engineered CO_2 stores. Geofluids,
605 15(3): 453-463. DOI:10.1111/gfl.12121

606 Schroder, I.F., Wilson, P., Feitz, A.F. and Ennis-King, J., 2017. Evaluating the performance
607 of soil flux surveys and inversion methods for quantification of CO_2 leakage. Energy
608 Procedia, 114: 3679-3694. DOI:10.1016/j.egypro.2017.03.1499

609 Schwarz, K.T., Patzek, T.W. and Silin, D.B., 2009. Dispersion by wind of CO_2 leaking
610 from underground storage: Comparison of analytical solution with simulation. International
611 Journal of Greenhouse Gas Control, 3(4): 422-430.

612 Shao, H., Ussiri, D.A.N., Patterson, C.G., Locke, R.A., Wang, H., Taylor, A.H. and Cohen,
613 H.F., 2019. Soil gas monitoring at the Illinois Basin - Decatur Project carbon sequestration
614 site. International Journal of Greenhouse Gas Control, 86: 112-124.

615 Werner, C., Fischer, T.P., Aiuppa, A., Edmonds, M., Cardellini, C., Carn, S., Chiodini, G.,
616 Cottrell, E., Burton, M., Shinohara, H. and Allard, P., 2019. Carbon Dioxide Emissions from
617 Subaerial Volcanic Regions: Two Decades in Review. In: B.N. Orcutt, I. Daniel and R.

618 Dasgupta (Editors), Deep Carbon: Past to Present. Cambridge University Press, Cambridge,
619 pp. 188-236.

620 West, J.M., Jones, D.G., Annunziatellis, A., Barlow, T.S., Beaubien, S.E., Bond, A.,
621 Breward, N., Coombs, P., de Angelis, D., Gardner, A., Gemeni, V., Graziani, S., Green, K.A.,
622 Gregory, S., Gwosdz, S., Hannis, S., Kirk, K., Koukouzas, N., Kruger, M., Libertini, S.,
623 Lister, T.R., Lombardi, S., Metcalfe, R., Pearce, J.M., Smith, K.L., Steven, M.D., Thatcher,
624 K. and Ziogou, F., 2015. Comparison of the impacts of elevated CO_2 soil gas concentrations
625 on selected European terrestrial environments. International Journal of Greenhouse Gas
626 Control, 42: 357-371. DOI:10.1016/j.ijggc.2015.07.020